EXPERIMENTAL STUDIES OF LOW ENERGY PROTON IRRADIATION OF THIN VACUUM DEPOSITED ALUMINUM LAYERS

Thomas Renger[1], **Maciej Sznajder**[2], **and Ulrich Geppert**[3]

[1]*DLR Institute for Space Systems, System Conditioning, Robert Hooke Str. 7, 28359 Bremen, Germany*
[2]*DLR Institute for Space Systems, University of Bremen, Robert Hooke Str. 7, 28359 Bremen, Germany*
[3]*DLR Institute for Space Systems, System Conditioning, Robert Hooke Str. 7, 28359 Bremen, Germany*
[3]*Kepler Institute of Astronomy, University of Zielona Góra, Lubuska 2, 65-265 Zielona Góra, Poland*

ABSTRACT

We present experimental studies of degradation effects caused by low energetic proton irradiation on thin Aluminum layers. The studies were performed by use the Complex Irradiation Facility (CIF) at the German Aerospace Center (DLR) in Bremen, Germany. Different proton doses and energies at two temperature levels of the samples were considered.

The result of the irradiation tests is a formation of bubbles at the Aluminum surface. They are filled with molecular Hydrogen gas, which is created by the recombination processes of the metal free electrons and the incident protons. The average size of the bubbles increases with higher proton doses. As a consequence of the effect the metallic surface morphology is changed significantly.

Key words: blistering; space environmental effects; complex irradiation facility; proton irradiation; Aluminum layer.

1. INTRODUCTION

Thin metallic films are widely used in space technology. Important applications are e.g. multilayer insulation blankets (MLI) or solar sails. These metallic films are exposed to a highly destructive environment under space conditions. In a sufficiently large distance from the Earth atmosphere, the solar wind and electromagnetic radiation are the dominating factors for material degradation, which will change their mechanical and thermo-optical properties.

Unfortunately, the real degradation behavior of materials in the interplanetary space is to a great extent unknown. Therefore, studies (both theoretical and experimental, carried out in terrestrial laboratories) are necessary to predict the expectable changes of the metallic film properties in order to plan long-term space missions. Especially a change of the surface morphology, which is attended to a decrease of its reflectivity, is influencing the efficiency of e.g. solar sail propulsion technology or the thermal control of MLI.

This paper is devoted to the particularly destructive aging effect caused by the low energy ($\leq$ 100keV) protons on 7.5 μm Polyamide foils (Upilex $-$ S$^{\textcircled{R}}$), covered on both sides with a 100 nm vacuum deposited Aluminum layer. The Hydrogen bubble formation is well studied [9]. It is one of the four general aging processes caused by Hydrogen (referred to as embrittlement)[6]. The presented experimental results are the first step to understand the true behavior of the bubble formation under real space conditions.

The paper is organized as follows. A short description of the CIF is given in Section 2. The theoretical background and the test parameters are explained in Section 3. The results of the experiments are discussed in Section 4. Finally, the conclusion is given in Section 5.

2. THE COMPLEX IRRADIATION FACILITY

The Complex Irradiation Facility (CIF) was designed and commissioned with the aim to perform material investigations under radiation conditions as prevalent in interplanetary space environment. Therefore three light sources and a dual beam irradiation system for the bombardment of the sample with electrons and protons are combined at a vacuum chamber for simultaneous irradiation. They cover the electromagnetic spectrum and the bulk of proton and electron fluxes of the solar wind with energies up to 100 keV. The light sources are an Argon-VUV-source, a Deuterium-UV-source, and a solar simulator with a Xenon lamp. The CIF can be used for a large variety of material studies. A great effort has been expended to simulate the radiation conditions as realistic as possible. It concerns especially the dimensioning of the electron and proton accelerator with respect to the energy and intensity range. It concerns as well the quality of the vacuum which can be achieved. That is an important aspect to detect material degradation because molecules of

the rest gas can interact with the radiation and degrade the surface of the sample and the results of the experiment would be distorted. Therefore the complete facility has been manufactured in UHV-technology with metal sealings and without organic compounds (no rubber vacuum sealings, oil-free pumps) to avoid this self-contamination.

2.1. Geometry and technical parameters

The CIF consists of a vacuum irradiation chamber (400 mm in diameter) which is connected to a lock chamber for the placement of the sample into the vacuum environment of the facility (see Fig. 1). The irradiation chamber has got four tubes with flanges for the connection with the radiation sources. They are arranged at an angle of 30 degrees to the neighboring one in the same level for the accelerator beam line, the solar simulator, and the Argon-VUV-source [14]. The Deuterium-UV-source is located above the solar simulator at an angle of 30 degrees between their axes. The axes of all radiation sources are crossing in the center of the irradiation chamber where the target station is mounted. The geometry of that arrangement, the target mounting, and the radiation sources itself are dimensioned in a way, that a square area of 80 mm can be irradiated simultaneously with all sources. The technical parameters of the CIF are summarized in Table 1.

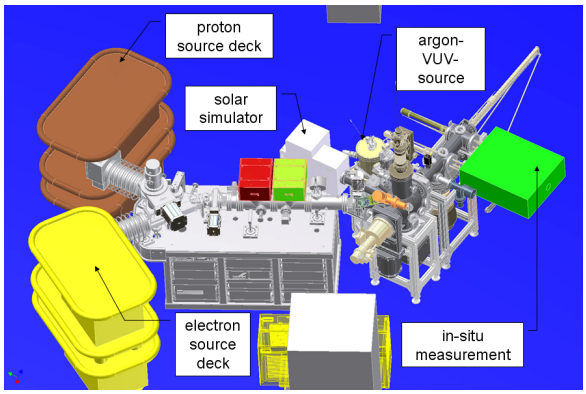

Figure 1. The CIF, electron and proton source deck are located on the left, solar simulator is in the center of the snap, Argon-VUV-source is located behind the chamber and the in-situ measurement on the right side of the chamber.

The sample mounted in a holder will be inserted into the lock chamber and transferred after vacuuming by a magnetic manipulator into the sample station of the irradiation chamber.

The vacuum system at the irradiation- and the lock chamber consists of a turbo molecular pump, an ion getter pump and a cryogenic pump to reach a pressure in the UHV-range. This will allow measurements with the quadrupole mass spectrometer which is installed at the irradiation chamber.

2.2. The Proton/Electron Dual Beam Irradiation System

The Dual Beam Irradiation System is designed to irradiate samples with protons or electrons independently or with both particle species simultaneously on a common axis. The selected beam(s) can be scanned over the samples. All relevant parameters can be adjusted remotely via the computer control system.

The vacuum system of the beam line consists of the acceleration tubes (one for each particle species), the dual inflection system, and the differential pumping segment. The dual inflection system is equipped with a turbo-molecular pump and the differential pumping segment with two ion getter pumps.

The protons are produced by ionization of Hydrogen, which is stored in a lecture bottle inside the source deck. After pressure reducing the Hydrogen is guided through a thermo-mechanical gas inlet valve with remote control to the ion source. The ionization takes place inside the glass bulb of the source by excitation with a radio frequency, which is capacitive coupled to the bulb. The plasma is confined and positioned by an axial permanent magnetic field. The source output is optimized by control of the source gas pressure and oscillator loading. There are not only positive ions H^+ (1 atomic mass unit) generated with Hydrogen gas, but also the molecule ions H_2^+ (2 atomic mass units) and H_3^+ (3 atomic mass units). This makes a mass selector necessary, which is installed in the dual inflection system (see below).

The electrons are generated by a lanthanum hexaboride (LaB_6) cathode, which is a high performance, resistively heated, thermionic electron source. A heater current and Wehnelt voltage control the electron current.

Both particle species are accelerated in appropriate tubes by a high voltage, which corresponds to the required energy. The acceleration tubes are manufactured as a metal to ceramic brazed assembly with no organic compounds. After the acceleration the beam(s) are deflected onto a common axis in the dual inflection system. This is realized by inflection magnets. The proton inflection magnet works additionally as a mass selector for the different ion species (elemental and molecular Hydrogen ions). The electron beam is magnetically shielded from the comparatively strong magnetic fields that are applied in the proton inflection line. Both the vertical and the horizontal position of each beam are adjusted by separate magnetic steerer, which are used to compensate the influence of the electron inflection magnet to the proton beam too. The negative influence of the magnetic components of the proton beam and/or the Earth magnetic field to the electron beam is corrected with special magnetic shielding techniques, compensating magnetic fields by correction coils and advanced software tools. A separate beam stopper for each particle species can be inserted pneumatically to block the beam while the other source is running. This is useful to tune each source separately.

Table 1. Technical parameters of the CIF.

vacuum test chamber	
volume	ca. 33.5 l (diameter: 400 mm)
irradiated target area	80 mm in diameter
vacuum pressure	down to 10^{-10} mbar in the empty chamber
thermal conditioning of the target	
heating	halogen spotlights from behind (600 W, max. 450°C)
cooling	liquid Nitrogen (IN_2: 80 K)
proton / electron dual beam irradiation system	
low energy range	1 - 10 keV, 1 - 100 nA
high energy range	10 - 100 keV, 0.1 - 100 μA
light sources	
solar simulator	250 - 2500 nm (5000 $\mathrm{Wm^{-2}}$)
Deuterium-UV-source	112 - 410 nm (1.65 $\mathrm{Wm^{-2}}$)
Argon-VUV-simulator	40 - 410 nm (50 $\mathrm{mWm^{-2}}$)
measurement instrumentation	
ex-situ-measurements	solar absorption, emissivity and reflectance
quadrupole mass spectrometer	range: $0 - 512$ amu
sensors	radiation, temperature and pressure

A retractable aperture can be inserted pneumatically into the beam at the differential pumping segment. It is used to reduce the current. If the current is adjusted it can be measured with the retractable Faraday cup. It can be inserted pneumatically in front of the scanning section. This must be done separately for each particle species, i.e. one beam must be blocked.

The electrostatic scanning segment contains two sets of deflection plates, which deflect the beam in two directions perpendicular to each other. The triangular voltages for these plates and its crystal locked frequencies are carefully chosen to eliminate the possibility of synchronization caused dose non-uniformity. The amplitude of the deflection voltages is adjusted by use of the Faraday cups, which are mounted at the corners of the sample station. They detect if the sample area is scanned completely.

3. FORMATION OF MOLECULAR HYDROGEN BUBBLES

H_2 bubbles are metal pockets filled with molecular Hydrogen gas resulting from recombination processes in the metal lattice. Solar wind protons, while penetrating the metallic target, recombine with its free electrons to neutral Hydrogen atoms. There are four recombination processes of ions into neutral atoms: the Auger process, the Resonant process, the Oppenheimer-Brinkman-Kramers process, and the Radiative Electron Capture process. Since the solar wind consists mainly of low-energetic protons ($\leq$ 100 keV), the Auger process leads the recombination. In that process, an electron is captured by the incident ion to a bound state assisted by an electron-hole pair [5, 10].

Blistering occurs as irradiation damage. Bubbles change the physical properties of the irradiated surface and increase the erosion rate [1]. It is known from terrestrial laboratory experiments that bubble caps lose thermal contact with the target body and, therefore, become overheated under intensive beams [1]. They can then crack and release the H_2-gas. Growth of bubbles on a flat surface can be interpreted as the increase of surface roughness that causes a decrease of reflectivity.

The tendency to form bubbles depends on: proton energy, time - integrated proton flux, temperature of the target, crystallographic orientation of the irradiated surface and on impurities and defects in the sample [4]. Hydrogen atoms are much smaller than metal ions, but they can introduce strain in a metal lattice when being absorbed as interstitial ions [8, 12, 13]. They can also change the electronic structure of near neighbor metal ions [12]. That causes an increase of the lattice energy. It may be decreased by the aggregation of the interstitial Hydrogen atoms into Hydrogen atom clusters, and then molecular Hydrogen bubbles [12]. Hydrogen could not agglomerate into H_2-clusters without the presence of vacancies in the metal lattice. The vacancy is a point defect in the lattice. It may be a dislocation or a missing ion [3]. Vacancies may be created by incident ions while penetrating the target metal. For Aluminum, numerical analysis performed with the SRIM software [15] have shown that a flux of 5 keV protons can induce 4 vacancies per one incident proton, while flux of 100 keV protons can induce up to 11 vacancies per incident proton. The final number of bubbles depends also on the number of vacancies initially placed in the metal lattice [9], i.e. it depends crucially on the production process of the metallic surfaces. A single vacancy in Aluminum can trap up to twelve H atoms. For comparison, a vacancy in Iron can trap only up to six H atoms [6].

Bubble formation takes place together with the so-called pitting formation. The pits are surface micropores that occur during proton irradiation of metals. The distribution of pits was found to be affected by particle energy,

total flux, crystal orientation, and crystal substructure [9]. The density of pits increases with decreasing energy of incident particles. Thus, even a perfectly produced metallic surface that contains no vacancies will acquire a certain surface roughness as soon as it is exposed to solar proton irradiation.

In summary there are two critical conditions that have to be fulfilled to initiate the bubble growth process at Aluminum surfaces. First the proton dose must exceed $\sim 10^{16}$ H^+ cm^{-2} [e.g. 9]. Second the temperature of the sample has to be high enough to start the bubble formation, but not too high to lose Hydrogen much too rapidly due to the high diffusivity of Hydrogen in metals. The range in which bubbles were observed is between 288 and 573 K [e.g. 4, 9].

3.1. Test parameters and corresponding space conditions

The test parameters for the first experiments were determined so that the both criterions regarding the temperature and the proton dose were fulfilled. The temperature was adjusted above the lower limit of the criterion to 300 and 323 K. The Temperature (T) of the foil as a function of the distance (d) from the Sun can be calculated by:

$$T = \left(\frac{A_\mathrm{a}}{A_\mathrm{e}} \frac{\alpha_\mathrm{S}}{\epsilon} \frac{H_\mathrm{Sun}}{\sigma_\mathrm{SB}} \right)^{\frac{1}{4}}, \qquad H_\mathrm{Sun} = \frac{1\ \mathrm{SC}}{d^2}. \qquad (1)$$

Here, A_a is the area of the sample which absorbs the electromagnetic radiation, while A_e is the area which emits the heat by radiation. Hence, the ratio $\frac{A_\mathrm{a}}{A_\mathrm{e}}$ equals 0.5. σ_SB is the Stefan-Boltzmann constant. The thermo-optical parameters have been provided by the manufacturer of the $\mathrm{Upilex-S}^{\circledR}$ foil, the UBE company. Solar absorptance α_S and thermal emittance ϵ are: 0.093 and 0.017, respectively. The temperature of the foil as a function of the distance from the Sun is represented by the solid line in Fig. 2. The red area (323 - 300 K) represents the temperature range at which the bubble formation has been confirmed by the experiments presented in this paper, see Section 4. That temperature range corresponds to a distance between 2.46 and 2.85 AU. The light-red area (570 - 300 K) is the temperature range at which the bubble formation is reported in the literature.

When a probe is irradiated in space, it collects incident ions from a wide energy range. The range depends on the type and the thickness of the irradiated material. The thinner the target material, the less ions stuck in it. Since above well defined critical energy (E_C) of protons they pass through the Al-layer, the 2.5 keV proton flux was chosen for the first experimental setup. With this energy all of the protons stuck in the 100 nm thick Aluminium (see Fig. 3, left plot). Therefore, side effects caused by $\mathrm{Upilex-S}^{\circledR}$ molecules and incident protons interactions are excluded. The critical energy was determined

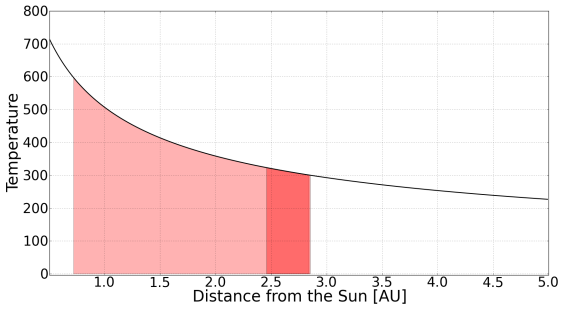

Figure 2. Temperature of the $\mathrm{Upilex-S}^{\circledR}$ *foil covered on both sides with 100 nm vacuum deposited Aluminum layer as a function of the distance from the Sun.*

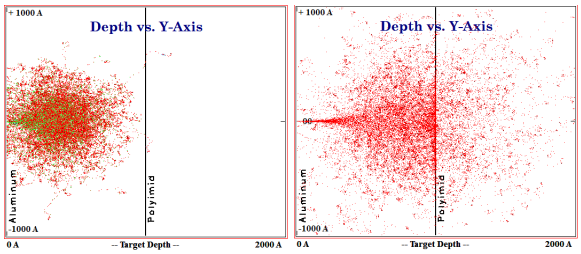

Figure 3. SRIM simulation of $\mathrm{Upilex-S}^{\circledR}$ *foil covered with 100 nm Al-layer irradiated by 2.5 (left) and 6.0 keV protons (right).*

by use of the SRIM software [15]. Figure 3 shows the simulation results for 2.5 and 6.0 keV. With 6.0 keV energy 32.8 % of the protons pass through the Al-layer.

The dose, which is defined as the number of protons per sample's unit area, was estimated as follows. The number of protons send to the target in an unit time (I), measured by the Farraday cup, multiplied by the irradiation time (t_i) and divided by the spot area (A) at the sample surface returns the expected dose.

$$D\ [p^+ cm^{-2}] = 6.24 \times 10^{12} \times \frac{I\ [\mu A]}{A\ [cm^2]} \times t_\mathrm{i}\ [s]. \qquad (2)$$

The retention time (t_S in Table 2) at a distance of 2.46 respectively 2.85 AU from the Sun according to the temperature levels, was calculated with the integral proton flux at these given orbits and the experimental dose. The integral flux was determined by use of the ACE (since 1997) database and converted from 1 AU to the appropriate distance.

The test parameters are summarized in Table 2.

Table 2. Test parameters

Probe symbol	T [K]	E [keV]	D [$\mathrm{p^+\ cm^{-2}}$]	t_S [days]
A1	300.0	2.5	4.3×10^{17}	3.5
A2	300.0	6.0	5.9×10^{17}	4.8
B1	323.0	2.5	7.8×10^{17}	4.8
B2	323.0	2.5	8.2×10^{17}	5.0
B3	323.0	2.5	1.3×10^{18}	7.9

4. RESULTS

The experiments have shown, that the bubble formation due to the Hydrogen recombination processes occurs in thin Al-layers. All samples shown in Table 2 were degraded. In this section the electron microscope measurements performed at the Foundation Institute of Materials Science (IWT), Bremen are presented.

The influence of the kinetic energy of incident protons to the surface morphology was examined. Fig. 4 shows the results of these studies for sample A1 (left) and A2 (right), which were irradiated with 2.5 and 6.0 keV, respectively (see Table 2). Clearly, only the sample A1 was populated by the bubbles. Sample A2 did not exhibit the bubble formation phenomenon. A reason could be, that the number of protons which pass through the Al-layer is to high (see Fig. 3). Small dark points seen on the picture are the pits i.e. small holes created due to proton irradiation. It is postulated, that through the holes the Polyimide foil is exposed. Note that both pictures are taken with different magnification.

The size of the molecular Hydrogen bubbles as a function of the proton dose has been investigated. Three probes (B1, B2, and B3) were exposed to a flux of 2.5 keV protons, each one with longer irradiation time, see Table 2. Results are shown in Fig. 5. From top to bottom, the pictures correspond to probes B1, B2, and B3, respectively. The average size of the bubbles has been estimated to 0.17 ± 0.05 μm, 0.2 ± 0.05 μm, and 0.25 ± 0.05 μm for probe B1, B2, and B3, respectively. Therefore, there is a strict correlation between the dose of protons and the average size of a bubble from the population.

Additionally, the surface morphology of probe B3 has been investigated by roughness measurements. Fig. 6 presents its surface height-profile. Three different positions have been pointed out (marked as red cross) to show the typical height of a bubble as well as a cavity which remain due to the proton irradiation.

5. CONCLUSIONS

It has been proven that molecular Hydrogen bubbles populate Aluminum surfaces under conditions that are prevalent in the interplanetary space, by the presented experimental results. The effect depends on the energy and the dose of the incident protons as well as the temperature of the target. These parameters were considered in the experimental setups. It has been shown that the change of morphology of a thin Al-layer depends strongly on the kinetic energy of the incident protons. The relation between the average bubble size and the proton dose was studied as well. As expected, samples which collected more protons were populated by bigger bubbles.

All samples were irradiated by mono-energetic protons. That situation does not reflect the real space conditions, since the solar wind consists of protons from a wide energy range. Therefore, quantitative predictions about the degradation behavior are not possible up to now.

These first experiments will be followed by further systematic investigations regarding more quantitative variations of proton energy and dose as well as different layer thickness. Furthermore the temperature limits of the effects have to be determined experimentally. Another topic is the influence of additional layers or coatings (e.g. silicon oxide).

REFERENCES

[1] Astrelin V. T. et al., 2009, Journal of Nuclear Materials 396, 43.

[2] Berger M. J., Coursey J. S., Zucker M. A., 2005, Stopping-Power and Range Tables for Electrons, Protons, and Helium Ions, NIST, Physical Measurement Laboratory.

[3] Damask A. C., Dienes G. J., 1971, Point Defects in Metals, Gordon and Breach.

[4] Daniels R. D., 1970, Journal of Applied Physics 42, 417.

[5] Guinea F., Flores F., Echenique P. M., 1982, Physical Review B 25, 6109.

[6] Lu G., Kaxiras E., 2005, Physical Review Letters 94, 155501.

[7] Linderoth S., 1988, Philosophical Magazine Letters 57, 229.

[8] Metzger H., Peisl J., Williams J., 1976, Journal of Physics F: Metal Physics 6, 2195.

[9] Milacek L. H., Daniels R. D., Cooley J. A., 1968, Journal of Applied Physics 39, 2803.

[10] Pauly N., Dubus A., Roesler M., 2002, Nuclear Instruments and Methods in Physics Research B: Beam Interactions with Materials and Atoms 193, 414.

[11] Polyanskiy. M. N., 2014, Refractive index database, http://refractiveindex.info.

[12] Ren X. et al., 2008, Materials Chemistry and Physics 107, 231.

[13] Tgomas G. J., Drotning W. D., 1983, Metallurgical Transactions A 8, 1545.

[14] Sznajder M. et al., 2013, Advances in Space Research 52, 1993.

[15] Ziegler J. F., 2014, SRIM software, www.srim.org

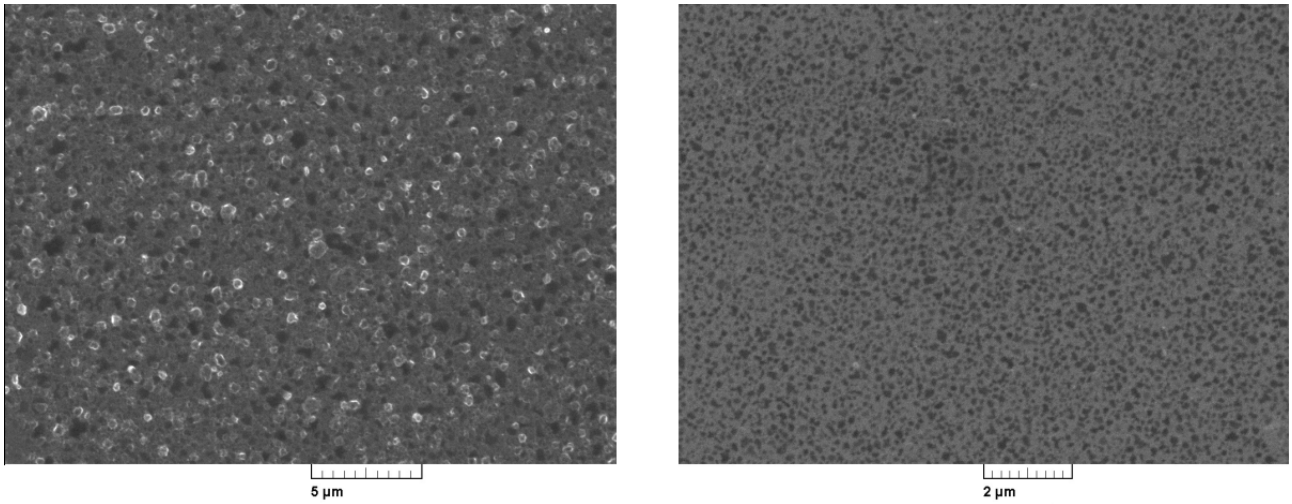

Figure 4. Electron microscope pictures of probes A1 (left) and A2 (right).

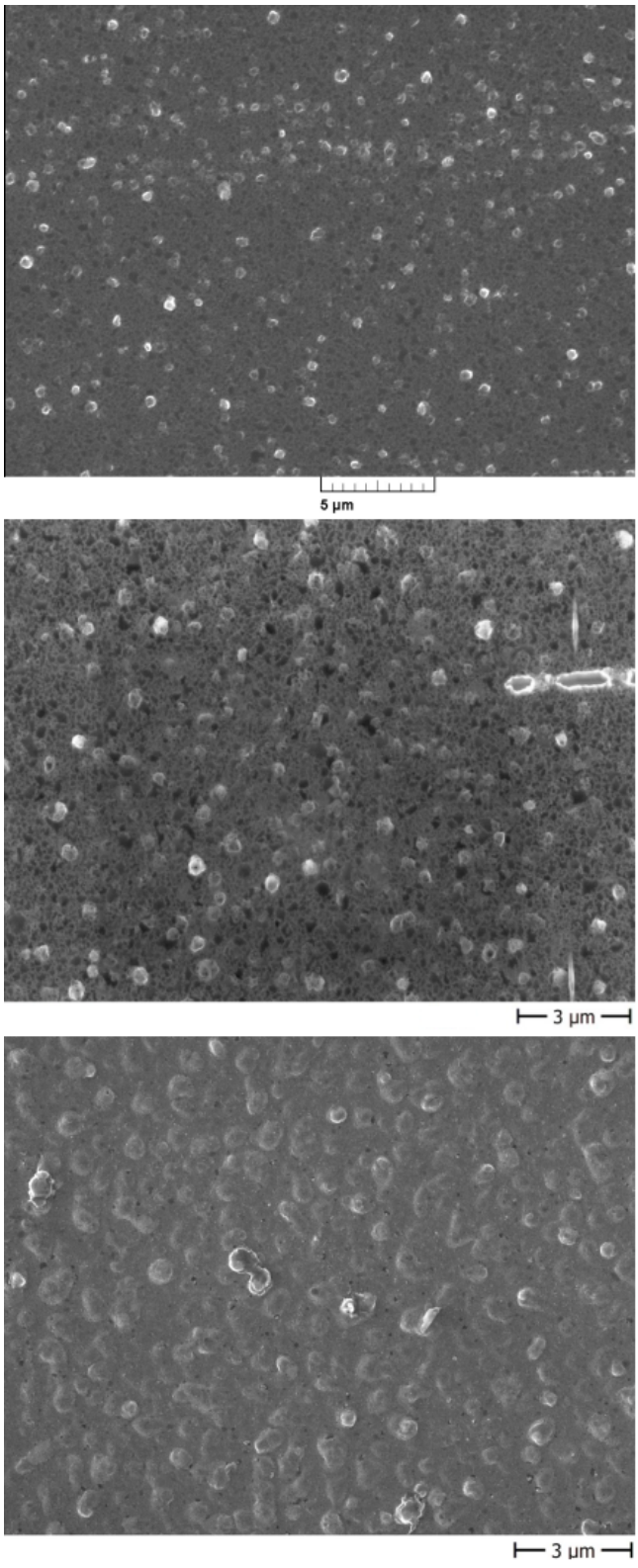

Figure 5. Electron microscope pictures of probes B1 (top), B2 (middle), and B3 (bottom).

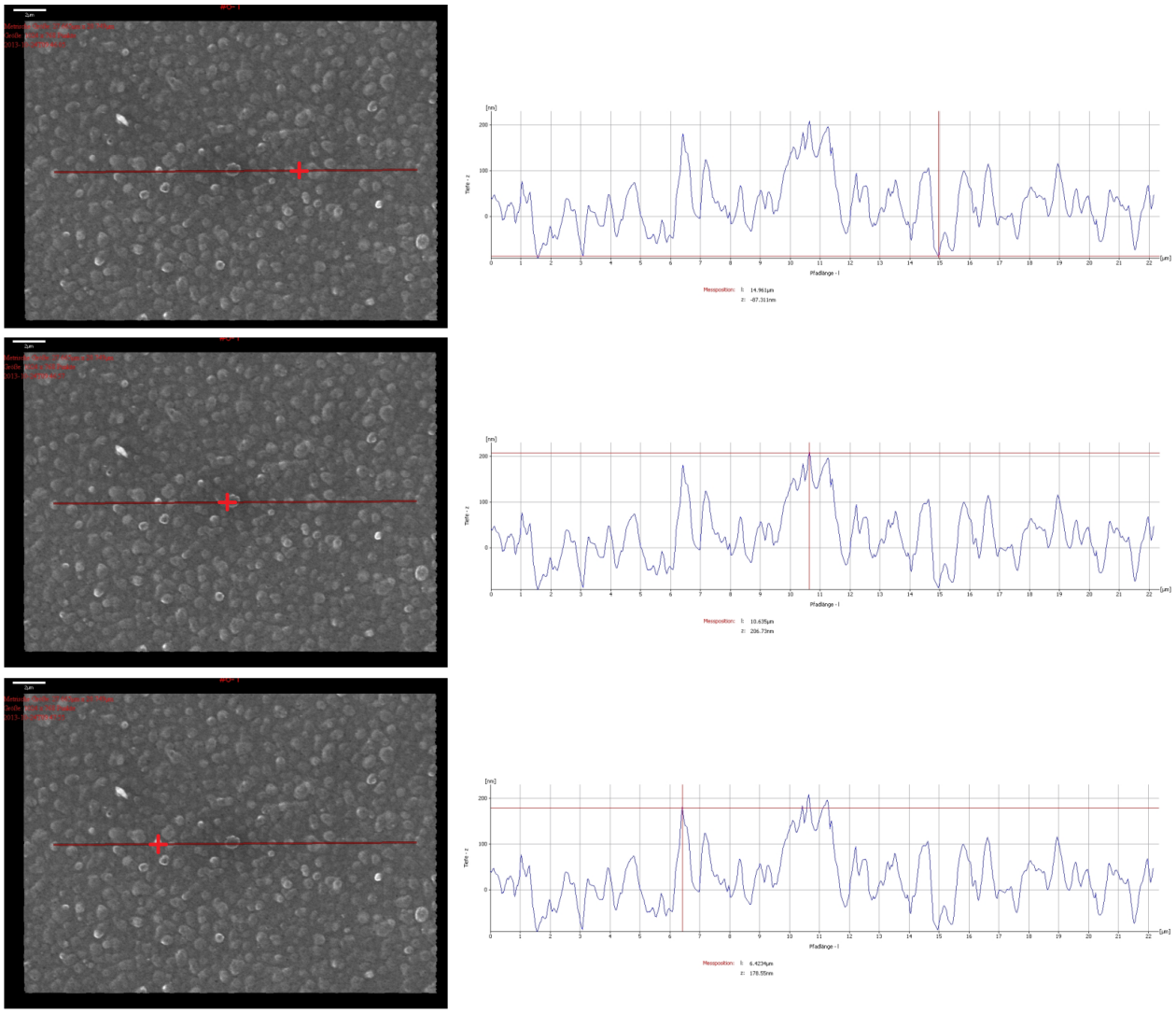

Figure 6. Three different positions on the probe B3 are shown. The top picture indicates a cavity on the surface, while the middle and the bottom pictures show the height of selected bubbles.